

Dielectric Relaxation and Solvation Dynamics in a Prototypical Ionic Liquid + Dipolar Protic Liquid Mixture: 1-Butyl-3-Methylimidazolium Tetrafluoroborate + Water

Xin-Xing Zhang,^{†,‡} Min Liang,[§] Johannes Hunger,^{||} Richard Buchner,^{||} and Mark Maroncelli^{*,§}

[†]Department of Physics, Nankai University, Tianjin, China

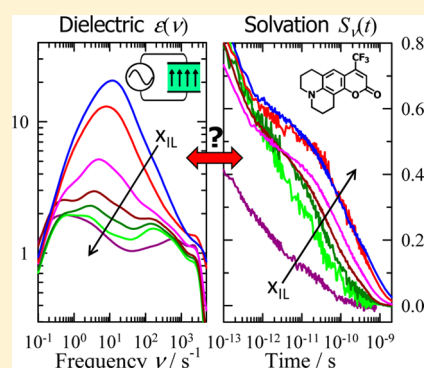
[‡]Department of Chemistry, Humboldt Universität zu Berlin, Germany

[§]Department of Chemistry, The Pennsylvania State University, University Park, Pennsylvania 16802, United States

^{||}Institut für Physikalische und Theoretische Chemie, Universität Regensburg, 93040 Regensburg, Germany

Supporting Information

ABSTRACT: Dielectric and solvation data on mixtures of 1-butyl-3-methylimidazolium tetrafluoroborate ([Im₄₁][BF₄]) + water are reported and used to examine the utility of dielectric solvation models. Dielectric permittivity and loss spectra (25 °C) were recorded over the frequency range 200 MHz to 89 GHz at 17 compositions and fit to a 4-Debye form. Dynamic Stokes shift measurements on the solute coumarin 153 (C153), made by combining fluorescence upconversion (80 fs resolution) and time-correlated single photon counting data (20 ns range), were used to determine the solvation response at 7 compositions (20.5 °C). All properties measured here were found to depend upon mixture composition in a simple continuous manner, especially when viewed in terms of volume fraction. Solvation response functions predicted by a simple dielectric continuum model are similar to but ~7-fold faster than the spectral response functions measured with C153. The solvation data are in better agreement with the recently published predictions of a semimolecular model of Biswas and co-workers [*J. Phys. Chem. B* **2011**, *115*, 4011], but these latter predictions are systematically slow by a factor of ~3.



1. INTRODUCTION

“Solvation dynamics”, the relaxation of solvation energy in response to perturbation of a solute, provides a window on liquid-state dynamics relevant to charge transport and charge-transfer, making this phenomenon of interest to applications in electrochemistry, energy-related fields, and synthesis.^{1–3} Solvation dynamics are most often measured by monitoring the time-resolved Stokes shift of a solvatochromic probe using spectroscopies such as transient absorption, fluorescence upconversion (FLUPS), and/or time-correlation single photon counting (TCSPC). Solvation by dipolar solvents has been studied for nearly half a century now,^{4–10} and many aspects, such as the connection to dielectric relaxation,^{11,12} are well characterized. With the widespread popularity of (room-temperature) ionic liquids as a new class of solvent and electrolyte over the past decade, recent focus has shifted to exploring solvation dynamics and its relationship to the dielectric behavior of ionic liquids.

The first studies of solvation dynamics in room-temperature ionic liquids¹³ are now already over decade old, and numerous groups have examined solvation and its relation to dielectric relaxation from experimental^{14–18} and modeling perspectives.^{19–25} Yet, it has only been in the past few years that both the requisite frequency and temporal coverage necessary for definitive tests of the relationship between solvation and dielectric relaxation have become available.^{26,25,27} Several groups

have been making dielectric measurements on neat ionic liquids in the megahertz to gigahertz range augmented by time domain terahertz.^{28–30} Recent solvation measurements have combined the techniques of Kerr gating^{31,32} and FLUPS,^{33,26,34} used for recording the subpicosecond response, with other methods that afford complete coverage out to nanosecond times. The similar behavior of the solvation response observed to the response predicted using dielectric data^{25,34} leaves little doubt that the two phenomena, and presumably the underlying solvent motions involved, are intimately related. However, in contrast to the case of dipolar liquids, in ionic liquids, dielectric continuum predictions are at least 2–4 times faster than the observed dynamics.³⁵ Some possible reasons for this discrepancy are discussed in ref 25.

To obtain additional perspective on the connection between solvation and dielectric relaxation, we have examined their relationship in mixtures of an ionic liquid, 1-butyl-3-methylimidazolium tetrafluoroborate ([Im₄₁][BF₄]) with the two dipolar solvents acetonitrile and water. These two mixtures, both showing complete miscibility at room temperature, were

Special Issue: Michael D. Fayer Festschrift

Received: May 2, 2013

Revised: May 22, 2013

chosen as illustrative of a prototypical ionic liquid interacting with prototype polar aprotic and hydrogen bonding solvents. Dielectric data on $[\text{Im}_{41}][\text{BF}_4]$ + acetonitrile have already been published³⁶ and solvation results will be reported separately.³⁴ Herein we present new data on the dielectric dispersion and loss of $[\text{Im}_{41}][\text{BF}_4]$ + water over the frequency range 200 MHz to 89 GHz together with fs+ps time-resolved measurements of the solvation dynamics of coumarin 153 (C153) for purposes of testing dielectric continuum models of solvation in ionic solutions.

A substantial body of literature is already available on ionic liquid + conventional solvent mixtures, and the $[\text{Im}_{41}][\text{BF}_4]$ + water mixture is one of the most thoroughly studied. Basic thermodynamic^{37,38} and physicochemical properties^{39–47} have been reported and reproduced by multiple groups. Rebelo et al.³⁷ reported an upper critical solution point at 4.4 °C and ionic liquid mole fraction $x_{\text{IL}} = 0.07$ (volume fraction $\Phi_{\text{IL}} = 0.44$). Early small-angle neutron scattering (SANS) studies suggested that the $[\text{Im}_{41}][\text{BF}_4]$ + water mixture contain small (~ 10 Å), polydisperse, water-rich spherical aggregates at concentrations above 0.8 M ($x_{\text{IL}} > 0.02$) at 25 °C.⁴⁸ Independent measurements of proton chemical shifts were similarly interpreted in terms of the presence of a critical aggregation concentration (CAC) in the range 0.7–1 M, and micelle-like structures were proposed based on these data.⁴⁹ However, the idea of aggregates with specific structures was questioned in a later SANS study,⁵⁰ which demonstrated that scattering and independent vapor pressure data³⁸ could be simultaneously described as resulting from random concentration fluctuations near to the critical point, rather than to surfactant-like aggregation. While most studies such as these are consistent with only molecular-scale structure existing at room temperatures, a recent light scattering study^{47,51} suggests that at near-critical compositions and 25 °C, a very small fraction of ions are contained in thermodynamically stable meso-structures with sizes of 200–800 nm.

A variety of spectroscopic methods have been employed to examine local structural features of the $[\text{Im}_{41}][\text{BF}_4]$ + water system. Most popular have been IR and Raman studies,^{52–58} sometimes augmented by ¹H NMR chemical shift measurements,^{54,57} both used to monitor water–water and water–ion hydrogen bonding. In many of these studies, discontinuous changes in the slopes of peak frequencies and relative intensities versus composition were interpreted in terms of “ice-like” water strongly bound to ions at low water content, which changes to water interacting predominantly with water at high water content. A number of other spectroscopic techniques, such as nuclear Overhauser effect (NOE) analysis,⁵⁹ near-infrared,⁶⁰ dielectric,⁶¹ far-infrared,^{62,63} and optical Kerr effect^{64,65} spectroscopies have also been applied.

Interpretation of such structural and spectroscopic data has been greatly aided by computer simulations undertaken by several groups.^{66,67,61,68–70} Moreno et al. simulated the $[\text{Im}_{41}][\text{BF}_4]$ + water system at 5 compositions ($x_{\text{IL}} \geq 0.5$) using two different all-atom representations.⁶⁶ Their primary interest was in comparing structural features observed in simulation to prior observations of component association deduced from early NOE data.⁵⁹ The simulations indicated that up to $x_{\text{w}} \sim 0.2$ water exists as isolated monomers and dimers and at higher water contents ($0.2 \leq x_{\text{w}} \leq 0.5$) as linear chains of increasing size. The distributions of contacts between specific cation–cation, water–cation, and water–anion nearest neighbor sites were found to differ slightly depending on the force field used, but to be generally consistent with experimental NOE data. As in the prior

NOE study, Moreno et al. interpreted the simulations to indicate significant hydrogen-bonding between the C2 hydrogen of the imidazolium cation and the oxygen of water.

In a series of three papers, Schröder and co-workers analyzed simulations of $[\text{Im}_{41}][\text{BF}_4]$ + water in the water-rich region.^{67,61,68} The first paper focused on radial distribution functions and the “collective networks” existing among the various components. Contrary to the conclusions of Moreno et al., Schröder et al. found no evidence for cation–water or cation–anion hydrogen bonding in these mixtures when applying conventional distance criteria for hydrogen bonding. They instead emphasized the strong hydrogen bonding present between BF_4^- and water, and the ionic network formed between the cation and anion.⁶⁷ The second paper in the series entailed comparison of experimental dielectric permittivity and loss data collected by some of the present authors to simulated counterparts.⁶¹ In this study, it was found that observed dielectric spectra could be approximately separated into contributions from water and cation reorientations and high-frequency cation + anion translational/vibrational motions. At the lowest water content studied, $x_{\text{IL}} = 0.2$, roughly equal contributions from these three types of motions were observed: a dominant and relatively distinctive peak due to water reorientation (10–20 GHz) and cation rotations and ion–ion translations/vibrations contributing primarily at lower and higher frequencies, respectively. In the third paper of the series, Schröder and co-workers performed a Voronoi analysis to rigorously associate system volumes with component species.⁶⁸ Among other things, this work highlighted the fact that the large size disparity between water and the ions of $[\text{Im}_{41}][\text{BF}_4]$ means that the ionic liquid component occupies more than half of the volume of the liquid for all $x_{\text{IL}} > 0.1$. For this reason, mole fraction provides a rather distorted measure of local environment in this system. Such volume considerations also highlight the error in envisioning distinct micelle-like aggregates with CAC values near 1 M where Φ_{IL} is ~ 0.5 .

Finally, Zhong et al. tested a recently developed united-atom force field against a variety of experimental data on the $[\text{Im}_{41}][\text{BF}_4]$ + water system.⁷⁰ In an impressive series of simulations spanning 12 compositions ($x_{\text{IL}} = 0–1$) and six different temperatures, Zhong et al. showed good to excellent agreement between their model’s predictions and experimental densities, mixing enthalpies, and viscosities. The simulations also offered a detailed view of the evolution of structure over the entire composition range. In agreement with Schröder et al., they found anion–water interactions to dominate over cation–water interactions. Snapshots of the simulated systems provide helpful perspective on the nature of ion and water aggregation in different concentration regimes. Analysis of radial distribution functions showed that ion–ion correlations (the “ionic network”⁶⁷) remain remarkably intact over the entire range $0.2 \leq x_{\text{IL}} \leq 1$. In water-rich systems ($x_{\text{IL}} \leq 0.2$) water was found to collect in large clusters containing hundreds of hydrogen-bonded molecules. As the ionic liquid content increases, these clusters are gradually broken down until by $x_{\text{IL}} \geq 0.8$ most water is either monomeric or in the form of clusters of 2–4 molecules. These structural changes were reflected in the simulated diffusion coefficients of water, which undergo changes in slope as a function of concentration at $x_{\text{IL}} = 0.2$ and 0.8, crudely dividing composition into regions of low, intermediate, and high ionic liquid content.

There have also been a number of studies of probe solvation in the $[\text{Im}_{41}][\text{BF}_4]$ + water system and related mixtures.^{71–76} Pandey and co-workers^{71–73} used a variety of solvatochromic

probes to determine Kamlet–Taft and other spectroscopic polarity parameters for $[\text{Im}_{41}][\text{BF}_4]$ + water and interpreted the nonlinear dependence of these parameters upon water mole fraction in terms of preferential solvation by the ionic liquid component.⁷² El-Seoud and co-workers⁷⁴ measured the absorption solvatochromism of four zwitterionic dyes and observed similar nonlinear shifts to the Pandey group. The latter workers analyzed their data in terms of solvation by water, ions, and ion + water complexes, and concluded that their probes are preferentially solvated by ion + water complexes. For reasons to be discussed in section 3C, we believe interpretations of this sort must be viewed with considerable caution.

Measurements of rotation times and dynamic Stokes shifts of fluorescent solutes have been used to probe solvation in mixed ionic liquid + conventional solvent systems.^{77–84} (We note that C153, the solute chosen for the present work, was used in all but the first of these studies.) Most relevant here are the early reports of Baker et al.⁷⁷ on $[\text{Im}_{41}][\text{PF}_6]$ + water and Sarkar and co-workers who studied $[\text{Im}_{41}][\text{PF}_6]$ ⁸³ and $[\text{Im}_{61}][\text{PF}_6]$ + water⁷⁹ mixtures. The more hydrophobic nature of PF_6^- compared to BF_4^- limited the range of compositions available in these mixtures to $x_w < 0.25$. At least in this low-water regime, solute rotation and solvation times were found to be approximately linear functions of solution viscosity. In these (and all but one other study⁸⁴), dynamic Stokes shifts were measured using techniques such that roughly half of the solvation response was faster than could be observed. Thus, only information about the slower portions of the response was available. Furthermore, suitable dielectric data on the mixtures were lacking, and it was therefore not possible to make comparison to dielectric continuum theories of solvation.

The topic of solvation dynamics in ionic liquid + conventional solvent mixtures has also been addressed in one computational⁸⁵ and one theoretical⁸⁶ report. Annapureddy et al. simulated C153 in $[\text{Im}_{61}][\text{PF}_6]$ + water at $x_w = 0.17$ in order to make direct comparison to the experiments of Sarkar and co-workers.⁷⁹ The simulations were able to reproduce the fact that the absorption and emission of C153 red-shift slightly in the presence of water. This study also showed that even this small amount of water greatly enhances the rate of solvent motions in the local vicinity of the solute. For an individual trajectory, relaxation in the presence of water appeared to be finished in ~ 300 ps compared to ~ 10 -fold slower relaxation in neat $[\text{Im}_{61}][\text{PF}_6]$. However, comparison of multiple trajectories revealed different apparent end points for the relaxation of different trajectories, indicating that the environmental exchange needed for complete relaxation occurs on longer time scales.⁸³ More recently, Daschakraborty and Biswas⁸⁶ described an approximate semimolecular theory of solvation in ionic liquid + conventional solvent mixtures. The theory assumes uncorrelated interactions between the solute and the ionic and dipolar components of the solution, and it uses as input experimental data on the dielectric response of the neat component liquids and the composition-dependent densities and viscosities of the mixtures. Explicit predictions for the extent of the dynamical Stokes shift of C153 and its time dependence in $[\text{Im}_{41}][\text{BF}_4]$ + water were provided in ref 86. These predictions will be compared to the experimental results generated here.

In the present paper we report new dielectric permittivity and loss measurements over the frequency range 200 MHz to 89 GHz and dynamic Stokes shift measurements of the solvation dynamics of C153 over times of 80 fs to 20 ns. This research is primarily aimed at testing the utility of simple dielectric continuum theories of solvation in ionic liquid + conventional

solvent mixtures. The data collected here also provide a more complete view of solvation in such a mixture than what has previously been available. After describing the experimental methods in section 2, the Results and Discussion is divided into five parts. Section 3.A describes the dielectric data. Section 3.B discusses these data in the context of other physical properties of the $[\text{Im}_{41}][\text{BF}_4]$ + water mixture relevant to solvation. Sections 3.C and 3.D describe the energetic and dynamical aspects of solvation of C153, and finally section 3.E concludes with comparisons of the observed solvation dynamics of C153 and the predictions of dielectric-based theories of solvation.

2. MATERIALS AND METHODS

2.A. Dielectric Measurements. The 1-butyl-3-methylimidazolium tetrafluoroborate ($[\text{Im}_{41}][\text{BF}_4]$) used for dielectric measurements was prepared from purified reactants as described elsewhere,⁴² yielding material with <150 ppm halide impurities (potentiometric titration against Ag^+). After drying under vacuum ($p < 10^{-8}$ bar) at $\sim 40^\circ\text{C}$ for at least 7 days, the water content was <40 ppm (coulometric Karl Fischer titration). Binary water + $[\text{Im}_{41}][\text{BF}_4]$ (IL) mixtures were prepared on an analytical balance. Water was deionized and purified with a Millipore Milli-Q system equipped with a $0.22\ \mu\text{m}$ filter. The dried compound was stored in a nitrogen-filled glovebox, and all measurements were conducted under an N_2 atmosphere. To minimize errors associated with the hydrolysis of BF_4^- , the samples were measured immediately after preparation. All dielectric experiments were performed at $25.00 \pm 0.05^\circ\text{C}$.

For all solutions, total complex permittivity spectra, $\hat{\eta}(\nu) = \eta'(\nu) - i\eta''(\nu)$, were measured as functions of frequency in the range $0.2 \leq \nu/\text{GHz} \leq 89$ by combining data obtained with a frequency-domain reflectometer ($0.2 \leq \nu/\text{GHz} \leq 20$)⁸⁷ and with two waveguide interferometers ($27 \leq \nu/\text{GHz} \leq 89$).⁸⁸ Raw frequency-domain reflectometer data, obtained using air, mercury, and water as the primary calibration standards, were corrected for calibration errors with a Padé approximation using pure propylene carbonate, dimethylacetamide, benzonitrile, and 1-butanol as secondary standards.⁸⁹ The interferometers do not require calibration. To account for the Ohmic loss of the samples, the static conductivities of the mixtures, σ , were determined to $\pm 0.2\%$ using an AC bridge and capillary cells, as described in detail elsewhere.⁴²

2.B. Spectroscopic Measurements. Coumarin 153 was purchased from Exciton and used as received. $[\text{Im}_{41}][\text{BF}_4]$ was obtained from Iolitec and dried under vacuum at 45°C overnight to <100 ppm water prior to sample preparation. Acetonitrile (anhydrous, spectrophotometric grade) was used as received from Sigma-Aldrich. Water was deionized and purified with a Barnstead Nanopure Diamond system. The mixtures were prepared by weight inside a nitrogen-purged glovebox.

Methods for collecting steady-state and time-resolved spectra are detailed in ref 27 and are not repeated here. Briefly, Hitachi U-3000 UV/vis and SPEX Fluorolog 212 spectrometers were used to collect electronic absorption and corrected⁹⁰ emission spectra in 1 cm path length quartz cuvettes. Time-resolved emission spectra with 25 ps resolution (fwhm of the instrument function) and 20 ns time windows were recorded using a TCSPC instrument based on Ti:sapphire laser excitation at 400 nm. Emission transients at 15–20 wavelengths were collected at 4 nm resolution and spectra reconstructed using the steady-state spectrum as a reference.⁹¹ Steady-state and TCSPC data were collected on samples thermostatted to $20.5 \pm 0.1^\circ\text{C}$. Time-resolved emission spectra (425–750 nm) with 80 fs resolution

and 650 ps time windows were collected using a FLUPS instrument recently described.⁹² An amplified Ti:sapphire laser + optical parametric amplifier provided excitation (400 nm) and gate (1340 nm) pulses at 500 Hz repetition rate. The samples were circulated through an optical cell of thickness 0.2–0.3 mm and kept from atmospheric water using Ar flushing as described in ref 27. C153 concentrations were chosen to provide optical densities of near 1 at 400 nm in a 1 mm cuvette. FLUPS measurements were conducted at room temperature, 20.5 ± 1 °C.

It should be noted that when making comparisons between the solvation and permittivity data collected, here we ignore the fact that the two data sets differ by 4.5 °C. As discussed in the Supporting Information, comparisons of viscosities measured at these two temperatures indicate that the errors incurred in doing so are negligible compared to the deviations between the observed solvation dynamics and the dielectric-based predictions.

3. RESULTS AND DISCUSSION

3.A. Dielectric Relaxation Data. Dielectric permittivity spectra

$$\hat{\epsilon}(\nu) = \epsilon'(\nu) - i\epsilon''(\nu) \quad (1)$$

were obtained from the measured complex permittivity spectra $\hat{\eta}(\nu)$ by correcting for the Ohmic loss contribution arising from direct current (dc) conductivity σ ,

$$\epsilon'(\nu) = \eta'(\nu), \quad \epsilon''(\nu) = \eta''(\nu) - \frac{\sigma}{2\pi\epsilon_0\nu} \quad (2)$$

with ϵ_0 the permittivity of free space. Representative permittivity and loss spectra are shown in Figure 1 (points). These spectra

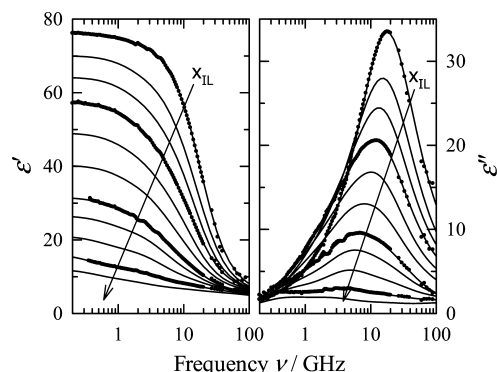


Figure 1. Sample dielectric permittivity $\epsilon'(\nu)$ and loss $\epsilon''(\nu)$ spectra of $[\text{Im}_{41}][\text{BF}_4]$ + water mixtures at 25 °C. Points are observed data, and lines are fits according to eq 3. Compositions in terms of IL mole fraction are 0.005, 0.019, 0.033, 0.050, 0.074, 0.11, 0.16, 0.20, 0.28, 0.49, and 0.89.

were modeled using a superposition of four Debye-type processes

$$\hat{\epsilon}(\nu) = \epsilon_\infty + \sum_{j=1}^4 \frac{S_j}{1 + 2\pi i\nu\tau_j} \quad (3)$$

where the S_j and τ_j are the relaxation strengths and times of the relaxation mode j , and ϵ_∞ is the high-frequency limiting permittivity. The smooth curves in Figure 1 are fits to this functional form. Table 1 provides the fit parameters for all of the compositions studied. The extrapolated static permittivity ϵ ,

given by $\epsilon = \epsilon_\infty + \sum S_j$, is also listed. It should be noted that the choice of simple Debye functions here may mean that contributions at times >1 ns are missed and thus ϵ is underestimated slightly at high values of x_{IL} , as the relaxation has been shown to broaden significantly at high x_{IL} and contain significant contributions above 1 ns.

All dielectric data can be well represented using eq 3 with time constants distributed across the range 1–300 ps. Whereas we do not attribute physical significance to the individual components of these fits, the limiting permittivities ϵ_∞ and ϵ , as well as the integral dielectric relaxation times $\langle\tau_{\text{diel}}\rangle = \sum_j S_j \tau_j / \sum_j S_j$, are relevant to solvation and are readily interpreted. These quantities are listed at the end of Table 1 and plotted in Figure S1. The static permittivity ϵ decreases monotonically (see Figure 2 below) from the value of 78 in water to 12.1 in neat $[\text{Im}_{41}][\text{BF}_4]$. (Previously reported values for neat $[\text{Im}_{41}][\text{BF}_4]$ are 11.7,⁹³ 13.9,⁹⁴ 14.6,⁹⁵ and 19.9.⁹⁶) The limiting high-frequency values ϵ_∞ vary erratically over the range 3.1–5.2, decreasing slightly with increasing IL content, presumably as a result of the decreasing importance of high-frequency components beyond the experimental range. Finally, the integral time $\langle\tau_{\text{diel}}\rangle$ increases substantially with ionic liquid content. This increase is roughly exponential with the ionic liquid volume fraction (see Figure S1.)

3.B. Other Physical Properties. Figure 2 illustrates the composition dependence of the static permittivity described above, as well as several other properties of relevance to solvation. Although mole fractions are more often reported in the literature, herein we describe composition using volume fraction, which we relate to mole fractions x_i by $\Phi_2(x_2) = x_2 \bar{V}_2 / (x_1 \bar{V}_1 + x_2 \bar{V}_2)$ using values of the component molar volumes $\bar{V}_{\text{IL}} = 188.2$ cm³/mol and $\bar{V}_{\text{water}} = 18.1$ cm³/mol.⁴⁵ As mentioned in the Introduction, the large disparity in the sizes of the ionic liquid ions compared to water causes a large difference in these two composition variables. The fact that volume fraction is a better indicator of local composition for purposes of discussing solvation is illustrated using refractive index (n_D) data in Figure 2. Here we plot n_D versus both volume fraction (points and linear fit) and mole fraction (dashed curve). Whereas n_D , as well as reaction field factors of the sort $(n_D^2 - 1)/(n_D^2 + 2)$, and ion concentrations relevant to solvation are all very nearly linear functions of volume fraction, these same quantities are highly nonlinear functions of mole fraction. Thus, we use volume fraction here and in the following section when discussing the energetics of solvation.

Collected data on properties related to solvation energies can be summarized by the fits

$$\epsilon = 78.27 - 30.95\Phi_{\text{IL}} - 108.0\Phi_{\text{IL}}^2 + 72.86\Phi_{\text{IL}}^3 \quad (4)$$

$$n_D = 1.331 + 0.890\Phi_{\text{IL}} \quad (5)$$

Despite the use of a cubic polynomial in eq 4, Figure 2 shows that the static dielectric constant is also approximately linear in Φ_{IL} . The same is not true of the transport properties most closely related to solute or solvation dynamics, the viscosity (η) and the conductivity (σ). The latter quantities can be fit to within the scatter of the collected data⁹⁷ by the functions

$$\ln(\eta/\text{mPa s}) = \frac{(-0.120 + 2.061\Phi_{\text{IL}} - 1.568\Phi_{\text{IL}}^2)}{(1 - 0.841\Phi_{\text{IL}} - 0.079\Phi_{\text{IL}}^2)} \quad (6)$$

and

Table 1. Parameters of Fits of $\hat{\epsilon}(\nu)$ Data to Eq 3

x_{IL}	Φ_{IL}	τ_1	S_1	τ_2	S_2	τ_3	S_3	τ_4	S_4	ϵ_∞	ϵ	$\langle\tau_{\text{diel}}\rangle$
0.0051	0.0503	284	1.38	68.5	2.57	8.96	65.39	1*	3.42	3.59	76.3	16
0.0088	0.0842	153	3.03	38.6	3.83	9.16	61.07	1.10	2.45	4.35	74.7	17
0.0193	0.170	109	5.47	24.1	11.46	9.12	46.57	1*	2.18	4.40	70.1	20
0.0330	0.262	124	5.57	36.2	10.07	10.49	41.72	0.87	3.54	3.35	64.2	25
0.0497	0.353	116	6.57	30.4	13.59	10.36	30.09	1*	3.30	3.79	57.3	28
0.0739	0.454	145	5.47	37.0	12.33	11.54	24.29	1.01	3.23	3.78	49.1	34
0.105	0.551	147	5.14	32.0	14.15	10.54	14.15	1.35	2.35	4.53	40.3	38
0.157	0.659	190	4.65	31.6	12.77	8.82	8.39	1*	0.60	5.19	31.6	52
0.199	0.721	217	3.99	33.1	10.83	8.63	5.73	1.36	1.58	4.46	26.6	58
0.283	0.804	280	3.76	35.4	7.84	7.36	3.51	1.06	2.07	3.97	21.2	79
0.414	0.880	384	3.96	42.0	4.94	8.51	2.81	0.83	2.83	3.08	17.6	121
0.492	0.910	431	3.98	43.7	4.29	7.37	2.16	1.03	2.22	3.62	16.3	152
0.575	0.934	418	3.41	47.7	3.71	8.03	1.90	1.12	2.15	3.70	14.9	145
0.684	0.958	369	2.87	52.8	3.13	8.96	1.63	1.12	2.24	3.57	13.4	126
0.759	0.970	333	2.73	53.8	2.81	8.36	1.50	1.02	2.20	3.46	12.7	116
0.893	0.989	355	2.90	58.2	2.39	8.60	1.26	1.05	2.10	3.46	12.1	137
1	1	478	3.17	72.11	2.2	12.14	1.18	1.03	2.18	3.34	12.1	194

x_{IL} and Φ_{IL} are the mole and volume fractions of $[\text{Im}_{41}][\text{BF}_4]$. Times τ_i and $\langle\tau_{\text{diel}}\rangle = \sum_j S_j \tau_j / \sum_j S_j$ are in ps. Asterisks indicate parameters fixed during the fitting procedure.

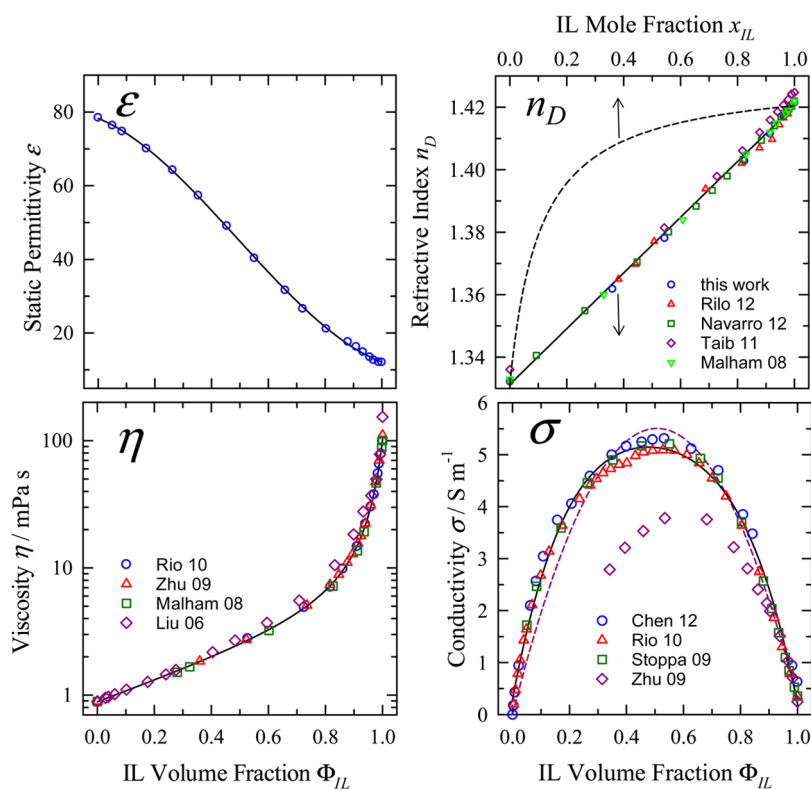


Figure 2. Some properties of the $[\text{Im}_{41}][\text{BF}_4]$ + water mixture measured at 25 °C in the present work and in previous studies.^{39–44,46} The solid curves are fits to the data as described in the text. In the conductivity plot, the solid curve is a fit to eq 7 and the dashed curve a fit to eq 8. The viscosity and conductivity fits exclude the deviant points labeled Rio 10 and Zhu 09, respectively.

$$\begin{aligned}
 (\sigma/\text{S m}^{-1}) = & 0.296 + 29.16\Phi_{\text{IL}} - 66.40\Phi_{\text{IL}}^2 + 72.68\Phi_{\text{IL}}^3 \\
 & - 35.54\Phi_{\text{IL}}^4
 \end{aligned}
 \quad (7)$$

The viscosity increases exponentially from $\eta_{\text{water}} \sim 1$ mPa s with Φ_{IL} up to $\Phi_{\text{IL}} \sim 0.6$ and then increases much more rapidly to values approaching those characteristic of ionic liquids. (As a function of mole fraction, the viscosity changes exponentially with x_{IL} for $x_{\text{IL}} > 0.2$ and more steeply before this point.) The conductivity is maximal near $\Phi_{\text{IL}} \sim 0.5$ ($x_{\text{IL}} \sim 0.1$), as is common in

ionic liquid + water mixtures.⁹⁸ We note that the conductivity data can be fit with some loss in accuracy using the simpler, theoretically based quadratic equation of Woodward and Harris:⁹⁸

$$\sigma = \Phi_{\text{IL}}(1 - \Phi_{\text{IL}})\sigma^0 + \Phi_{\text{IL}}^2\sigma_{\text{IL}} \quad (8)$$

with $\sigma^0 = 21.7 \text{ S m}^{-1}$ and $\sigma_{\text{IL}} = 0.29 \text{ S m}^{-1}$ (dashed curve in Figure 2).

3.C. C153 Solvation Energies. The electronic absorption and emission spectra of C153 at all compositions are broad and featureless and, apart from a frequency shift, comparable to the spectra in the neat $[\text{Im}_{41}][\text{PF}_6]$. As shown in Figure 3(a,b), both

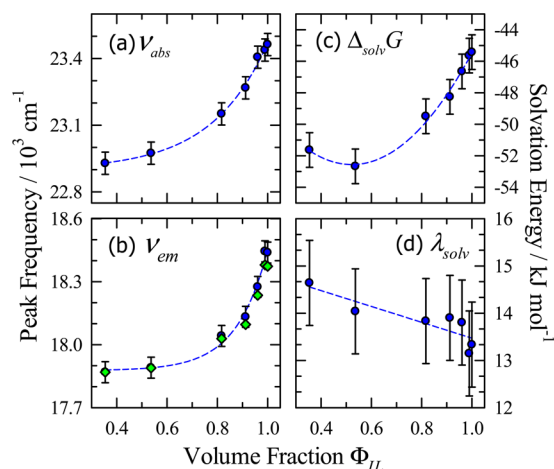


Figure 3. Peak frequencies of the $S_0 \leftrightarrow S_1$ absorption (a) and emission (b) and associated solvation energies (c,d; eqs 9 and 10) of C153 in the mixture. In panel b, blue circles denote steady-state emission frequencies and green diamonds denote frequencies extrapolated to long times $\nu(\infty)$ from time-evolving emission spectra.

the absorption and emission spectra are red-shifted by $\sim 550 \text{ cm}^{-1}$ in the mixture with the highest water content studied, $x_{\text{IL}} = 0.05$, $\Phi_{\text{IL}} = 0.35$. (C153 is insufficiently soluble in water to obtain reliable spectra at the neat water limit; the present data extrapolate to $\nu_{\text{abs}} \sim 22,900$ and $\nu_{\text{em}} \sim 17,880 \text{ cm}^{-1}$.) The frequency shifts appear to be monotonic but nonlinear in volume fraction.

As in previous work,^{16,27} we use absorption and emission frequencies to determine two solvation quantities: the solvent contribution to the free energy difference $\Delta_{\text{solv}}G$ and the reorganization energy λ_{solv} associated with the $S_0 \leftrightarrow S_1$ transition of C153:

$$\Delta_{\text{solv}}G = \frac{1}{2}h[\nu_{\text{abs}} + \nu(\infty)] - \Delta G_0 \quad (9)$$

$$\lambda_{\text{solv}} = \frac{1}{2}h[\nu(0) - \nu(\infty)] \quad (10)$$

In these equations ν_{abs} , $\nu(0)$, and $\nu(\infty)$ represent some measure of the frequency of the absorption, “time-zero” emission,⁹⁹ and the fully equilibrated emission, respectively, and ΔG_0 is the estimated gas-phase energy difference (see ref 27 for details). Unlike the frequencies themselves, which are of mixed origin, λ_{solv} represents the interaction of only the nuclear solvent polarizability, and $\Delta_{\text{solv}}G$ the interaction of the total (nuclear plus electronic) solvent polarizability with the solute electronic transition. As far as this C153 transition is concerned, both the total and nuclear polarizabilities of water (or the most dilute IL solution) are greater than those of $[\text{Im}_{41}][\text{BF}_4]$. However, the range of values observed in these mixtures is modest, only $\sim 13\%$ of the total energies in both cases. The reorganization energy is an approximately linear function of volume fraction, whereas the free energy exhibits a minimum near $\Phi_{\text{IL}} \sim 0.5$ (Figure 3), where the conductivity is maximal (Figure 2).

It is common to try to interpret data like those shown in Figure 3 in terms of solvation structure and preferential solva-

tion.^{100,101,72} For example, the fact that the frequencies ν_{abs} and ν_{em} change much more rapidly when a small amount of water is added to the neat ionic liquid compared to when $[\text{Im}_{41}][\text{BF}_4]$ is added to water might suggest preferential solvation of C153 by water. However, such interpretations, especially in the case of an ionic liquid + water mixture, are fraught with ambiguity. One problem is the fact that the disparate sizes of water and ionic liquid ions renders the appearance of plots like those in Figure 3 strongly dependent upon the choice of composition variable. We illustrate this point in Figure 4, where we replot ν_{abs} and ν_{em} of

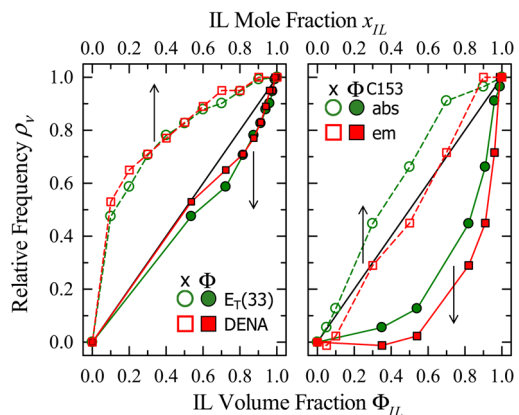


Figure 4. Illustration of the differences between mole and volume fraction representations of spectroscopic data. Data in the left panel are from absorption frequencies of the $E_T(33)$ dye and DENA from Sarkar et al.⁷² Spectral frequencies are plotted using the relative frequency format of eq 11.

C153 as functions of both volume and mole fraction (right panel). For comparison, the left panel contains absorption frequency data for two probes, “ $E_T(33)$ ” a water-soluble variant of Reichardt’s dye,¹⁰² and the π^* polarity indicator *N,N*-diethyl-4-nitroaniline (DENA) taken from the multiprobe study by Sarkar et al.⁷² All data in Figure 4 are plotted in terms of relative frequency

$$\rho_v = \frac{\nu - \nu_w}{\nu_{\text{IL}} - \nu_w} \quad (11)$$

where ν_w and ν_{IL} are frequencies in the pure water and ionic liquid limits. The straight lines in Figure 4 indicate what might be thought of as “ideal” mixing behavior, i.e., the case wherein probe frequencies vary linearly with mixture composition between the neat solvent limits. In the case of the $E_T(33)$ and DENA probes, a mole fraction representation shows strong positive deviations from ideality, whereas negligible or slightly negative deviations are found when these same data plotted versus volume fraction. The C153 frequencies show just the opposite behavior. The conclusion that $E_T(33)$ and DENA are preferentially solvated by water⁷² or that C153 is preferentially solvated by ions depends upon whether one chooses x_{IL} or Φ_{IL} to represent composition. As already discussed, we contend that the fact that dielectric quantities n_D and ϵ (Figure 2) as well as dipole and ion densities are linear or nearly linear functions of Φ_{IL} makes this variable the better choice. Nevertheless, given the cooperative nature of electrostatic interactions,¹⁰³ in the absence of an accurate theory of solvation in ionic solutions, it is not safe to assume that local compositions can be inferred from either type of plot. In the present case, choice of Φ_{IL} would lead to the conclusion that C153 is preferentially solvated by water. Such a conclusion is

contrary to the fact that C153 is much more soluble in $[\text{Im}_{41}][\text{BF}_4]$ than in water. Additional simulations of the sort performed by Annapureddy et al.⁸⁵ are required to adequately interpret these spectral shifts.

3.D. The Solvation Response. Representative time-resolved emission spectra of C153 ($x_{\text{IL}} = 0.5$; $\Phi_{\text{IL}} = 0.91$) recorded using FLUPS and time correlated single photon counting (TCSPC) are shown in Figure 5. As detailed in ref 27,

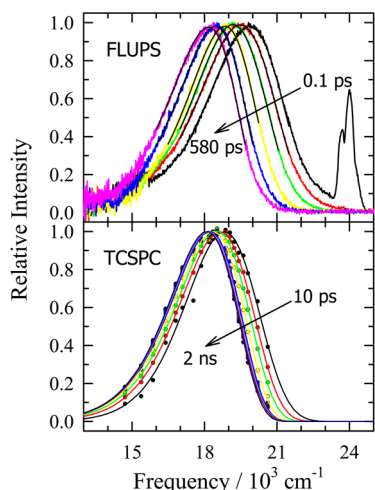


Figure 5. Representative time-resolved emission spectra of C153 in the $x_{\text{IL}} = 0.5$ ($\Phi_{\text{IL}} = 0.91$) mixture. The top panel show FLUPS data (noisier curves) and the lower panel spectra reconstructed from TCSPC decays (points). The smooth curves in both cases are log-normal fits of the data used for analysis. The spike near 24,000 cm^{-1} in the earliest FLUPS spectrum is due to Raman scattering.

such spectra are fit to log-normal line shape functions, and the resulting fit parameters are spliced together at intermediate times to obtain the full spectral evolution over times of 100 fs – 20 ns. The peak frequencies $\nu_{\text{pk}}(t)$ from such fitted data are used to determine the spectral or solvation response function

$$S_{\nu}(t) = \frac{\nu_{\text{pk}}(t) - \nu_{\text{pk}}(\infty)}{\nu_{\text{pk}}(0) - \nu_{\text{pk}}(\infty)} \quad (12)$$

The values $\nu_{\text{pk}}(0)$ and $\nu_{\text{pk}}(\infty)$ are obtained from steady-state spectra⁹⁹ and from extrapolating fits of TCSPC data beyond 20 ns, respectively.

Spectral response functions of C153 are shown in Figure 6. As in neat ionic liquids,²⁷ $S_{\nu}(t)$ in these mixtures consist of a fast subpicosecond component and a broadly distributed slow component. The latter relaxes over times between a few picoseconds to a few nanoseconds. With the exception of the $x_{\text{IL}} = 0.05$ mixture, the fast component, assignable to inertial ion and water motions, accounts for about one-third of the response, and the slower diffusive motions account for the rest. In the $x_{\text{IL}} = 0.05$ case and in pure water (represented in Figure 6 by data on the water-soluble probe coumarin C343¹⁰⁴), subpicosecond dynamics account for more than half of the response.

To characterize the fast and slow components of $S_{\nu}(t)$ we fit these data to both Gaussian + stretched exponential and triple exponential functions of time. Details are provided in the Supporting Information. Figure 7 shows fitted values of the fast (τ_f), slow (τ_s), and overall integral times (τ_{solv}) plotted as functions of solvent viscosity. At least to within the large experimental uncertainties ($\pm 40\%$), the fast time τ_f shows no

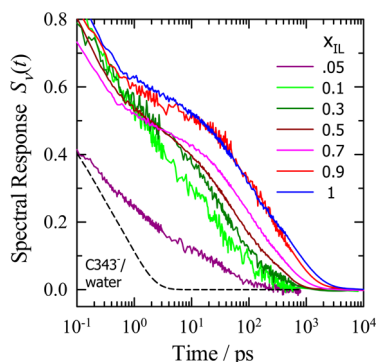


Figure 6. Spectral response functions (eq 12) of C153 at seven mixture compositions. The dashed line is the result previously reported for the probe C343¹⁰⁴ in pure water.

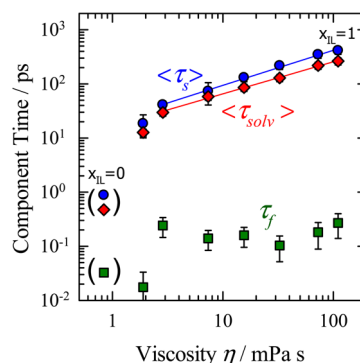


Figure 7. Times associated with the solvation response of C153 plotted as functions of solution viscosity. τ_f , τ_s , and τ_{solv} are the fast, slow, and overall integral times of $S_{\nu}(t)$. Values in parentheses are data on C343¹⁰⁴ in pure water from ref 104. The lines through the τ_s and τ_{solv} data, for $x_{\text{IL}} \geq 0.1$ the times are proportional to η^p with $p \sim 0.6$. This dependence upon viscosity is weaker than what is observed in neat ionic liquids where $p \sim 1$.^{16,27} Not shown in Figure 7 is the fact that over the range $0.1 \leq x_{\text{IL}} \leq 0.5$, the slow solvation times $\langle \tau_s \rangle$ are close to the integral dielectric times $\langle \tau_{\text{diel}} \rangle$.

systematic variation with viscosity or mixture composition over the range $0.1 \leq x_{\text{IL}} \leq 1$. However, at $x_{\text{IL}} = 0.05$ ($\Phi_{\text{IL}} = 0.35$), τ_f decreases to a value comparable to that expected in pure water. The slow component, and with it the overall correlation time, varies significantly with composition and viscosity over the full composition range. As illustrated by the lines drawn through the $\langle \tau_s \rangle$ and $\langle \tau_{\text{solv}} \rangle$ data, for $x_{\text{IL}} \geq 0.1$ the times are proportional to η^p with $p \sim 0.6$. This dependence upon viscosity is weaker than what is observed in neat ionic liquids where $p \sim 1$.^{16,27} Not shown in Figure 7 is the fact that over the range $0.1 \leq x_{\text{IL}} \leq 0.5$, the slow solvation times $\langle \tau_s \rangle$ are close to the integral dielectric times $\langle \tau_{\text{diel}} \rangle$.

We recently showed dielectric continuum models predict integral solvation times in conducting solvents should be proportional to solution resistivity, σ^{-1} , where σ is the static conductivity.^{105,35} We also found that σ^{-1} is a better empirical predictor of solvation times in ionic liquids than is viscosity.³⁵ Figure 8 examines this connection in the present mixture. The solid line in Figure 8 shows the correlation established for solvation of C153 in 34 ionic liquids near room temperature; the shaded region indicates 95% confidence limits for prediction in neat ionic liquids. None of the mixture data fall outside of the latter limits. However, the curvature in the data results from the fact that there is a maximum in conductivity (Figure 2) whereas the solvation times increase monotonically with composition. Thus, the relationship between $\langle \tau_{\text{solv}} \rangle$ and σ^{-1} does not appear to describe the behavior of this mixture, at least not over the entire composition range.

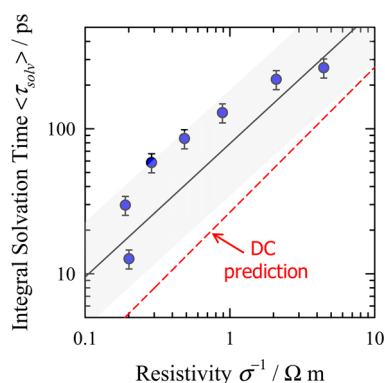


Figure 8. Integral solvation times plotted versus solution resistivity. The solid line and shaded region indicate the correlation established in neat ionic liquids³⁵ and the 95% prediction region of this fit, respectively. The dashed line labeled “DC prediction” is the result of a simple dielectric continuum model.¹⁰⁵

3.E. Connecting Dielectric Relaxation and Solvation Dynamics. We finally consider use of solvation models for understanding the connection between the dielectric dispersion of these mixtures and the time-dependence of C153 solvation. The simplest connection is afforded by the dielectric continuum model, which assumes the solute to be a sphere possessing a centered point dipole and polarizability (represented by a cavity dielectric constant $\epsilon_c = 2$) and the solvent to be fully characterized by the permittivity function $\hat{\eta}(\nu)$. We will make the comparison between $S_\nu(t)$ and $\hat{\eta}(\nu)$ within this simple model from two perspectives.

First we use the parametrized $\hat{\eta}(\nu)$ from Table 1 to predict $S_\nu(t)$. Details of how these calculations are performed are described in refs 27 and 35, and will not be repeated here. One issue that must be addressed when performing such calculations is the fact that dielectric measurements to 89 GHz do not capture all of $\hat{\eta}(\nu)$ needed to accurately predict the early portion of solvation. Data at sufficiently high frequencies (10 and 3 THz, respectively) is available for the neat solvents water¹⁰⁶ and $[\text{Im}_{41}][\text{BF}_4]$.²⁸ To approximate the effects of the missing high-frequency portions of the spectra in the mixtures, we used a volume-fraction-weighted average of the pure component spectra as described in the Supporting Information. Comparisons with the terahertz data of Koberg et al.⁶³ (Figure S6) suggest that this approximation is reasonably accurate. Nevertheless, this approximation renders the predictions of the solvation response at short times (<1 ps) less certain than those at longer times, which should be accurately reproduced.^{25,27}

The solvation response functions $S(t)$ predicted from permittivity data are shown in Figure 9. Except for the $x_{\text{IL}} = 0.05$ mixture, these $S(t)$ functions are similar in appearance to the observed functions, $S_\nu(t)$, in Figure 6. (Some direct comparisons are provided in Figure S7.) At most compositions, the relative amplitude of the fast and slow components and the broadly distributed character of the slow component are approximately reproduced by the continuum model, but the predicted functions are shifted to shorter times. In the most dilute mixture, the observed decays (Figure 6) indicate that a large fraction of the response is faster than can be resolved in the FLUPS experiments (<100 fs), as is the case in pure water. In contrast, the dielectric predictions for $x_{\text{IL}} = 0.05$ in Figure 9 suggest a much slower ultrafast component and a rather different time-dependence in the observable time window.

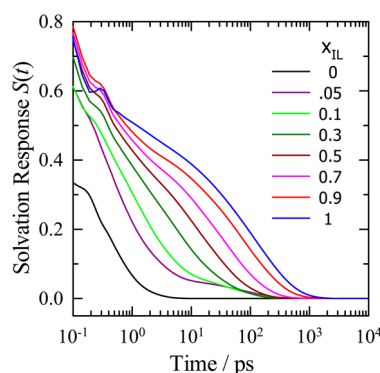


Figure 9. Solvation response functions calculated based on dielectric dispersion and conductivity data and a simple dielectric continuum model of solvation.

In Figure 10 we quantify the differences between the observed and predicted responses by comparing the times t_f required for

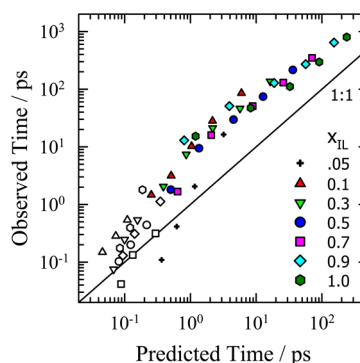


Figure 10. Comparison of the times t_f required for the observed ($S_\nu(t)$) and predicted ($S(t)$) response functions to reach levels $S(t_f) = f$ with $f = 0.8, 0.7, \dots, 0.2, 0.1$. (In the case of $x_{\text{IL}} = 0.05$, only $f \leq 0.4$ is observed and plotted.) Colored symbols indicate levels for which $f \leq 0.5$.

the respective functions to reach levels $S(t_f) = f$ with $f = 0.8, 0.7, \dots, 0.2, 0.1$. Comparisons are most reliable for observed times greater than 1 ps or $f \leq 0.5$, and these data are indicated by the colored points in Figure 10. For this slower portion of the response, apart from the $x_{\text{IL}} = 0.05$ data, the observed times are on average a factor of 7 larger than the predictions. The difference between the two times tends to increase systematically with decreasing x_{IL} . For example, at the smallest values of $f = 0.1$ and 0.2 , the ratios of observed to calculated times are: 3.3, 4.5, 5.0, 5.9, 8.3, and 14 at $x_{\text{IL}} = 1, 0.9, 0.7, 0.5, 0.3$, and 0.1 , respectively. In general, the deviations between observed and predicted solvation response functions in this $[\text{Im}_{41}][\text{BF}_4]$ +water system are similar to, but somewhat larger than, what we previously reported for a variety of neat ionic liquids.²⁷

An alternative perspective on the simple continuum model can be obtained by inverting observed $S_\nu(t)$ data to infer “effective” dielectric spectra reported by the solute, as described in ref 105. Briefly, the $S_\nu(t)$ data are refit to a 4-exponential form and the fit parameters used to determine $\hat{\eta}_{\text{eff}}(\nu)$, which is assumed to be of the form

$$\hat{\eta}_{\text{eff}}(\nu) = \epsilon_\infty + \sum_{j=1}^3 \frac{S'_j}{1 + 2\pi i \nu \tau'_j} + \frac{i\sigma_{\text{eff}}}{2\pi\epsilon_0\nu} \quad (13)$$

(The primes here are meant to distinguish the present parameters from those used in eqs 1–3 used to describe the measured $\hat{\eta}(\nu)$ data.) Given the constraint $S_\nu(0) = 1$, a 4-exponential representation of $S_\nu(t)$ provides seven independent parameters, which serve to uniquely determine the parameter set $\{S'_j, \tau'_j, \sigma_{\text{eff}}\}$ in eq 13 when the experimental value of n_D^{105} is used for ϵ_∞ . Results of such an analysis are presented in Figures 11 and 12.

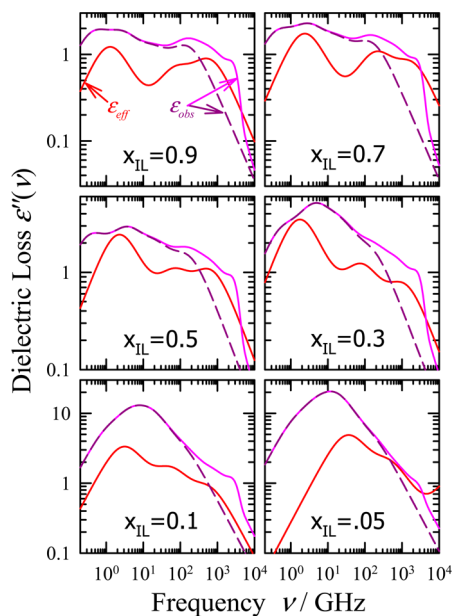


Figure 11. Observed (dashed purple and solid pink curves) and effective (red) dielectric loss spectra determined from $S_\nu(t)$ data as described in the text. The dashed purple curves are from parametrized fits to bulk dielectric data extending to 89 GHz, whereas the solid pink curves have been approximately corrected for missing high-frequency components as described in the Supporting Information. In all cases, the diverging conductivity term has been subtracted from the spectra.

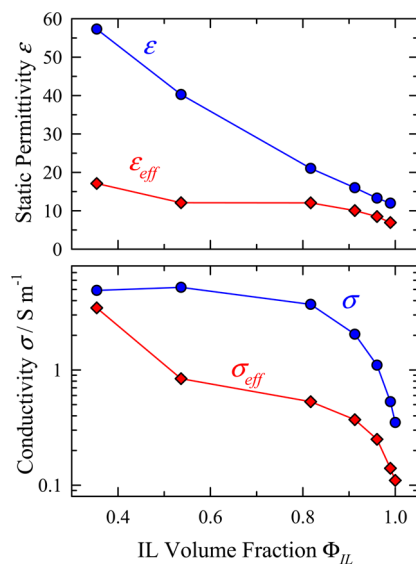


Figure 12. Comparison of the observed dielectric parameters ϵ and σ and their effective values derived from the solvation dynamics data.

Figure 11 compares $\epsilon''(\nu)$ spectra, the imaginary portion of $\hat{\eta}(\nu)$ after removal of the diverging final term of eq 13. Although the details of the experimental spectra are not reproduced, with

the exception of the $x_{\text{IL}} = 0.05$ mixture, there is a reasonable correspondence between the breadths and shapes of the effective loss spectra and their observed counterparts. The amplitudes of $\epsilon''_{\text{eff}}(\nu)$ are, however, systematically below those of the measured spectra. The difference is better illustrated in the top panel of Figure 12, where the static permittivity $\epsilon = \epsilon_\infty + \sum_j S_j$ is used as a measure of the overall “dielectric strength” in the spectra. Ignoring the $x_{\text{IL}} = 0.05$ data, the value of ϵ measured in bulk dielectric measurements is an average of 2.0 times larger than the effective value ϵ_{eff} obtained from inverting the solvation data. The bottom panel shows that the effective conductivity values obtained in this manner depart even more substantially from bulk measurements, by an average of a factor of 5.0. The fact that the general shapes of the effective and measured loss spectra are similar but the values of ϵ and σ differ significantly parallels the fact that the observed and predicted $S(t)$ curves have close to the same shape but are displaced in time in the semilog representations of Figures 6 and 9. One can either view these differences as reflecting failure of the dielectric continuum model as a quantitative description of solvation or as an indication that the effective properties of the solvent near to the solute differ substantially from their bulk values. In the latter case, one might conclude that C153 feels a dielectric environment closer to that of the neat ionic liquid than that of the bulk solvent.

A final comparison afforded by the present data is to the approximate semimolecular description of solvation of Biswas and co-workers.^{107,108} This theory combines experimental $\hat{\epsilon}(\nu)$ and viscosity data with information concerning solvent and solvation structure based on hard-sphere liquid models in order to approximately account for molecular aspects of solvation missing from the dielectric continuum model. Daschakraborty and Biswas⁸⁶ recently made predictions for solvation of C153 in $[\text{Im}_{41}][\text{BF}_4]$ + water, which may be directly compared to our experimental data. Figure 13 displays this comparison both for solvation energies (λ_{solv} , top panel) and characteristic times of the solvation response (bottom panel). Considering energies first, Figure 13 shows that this theory predicts a roughly 2-fold difference between the solvent reorganization energy in water compared to $[\text{Im}_{41}][\text{BF}_4]$, in contrast to the near composition

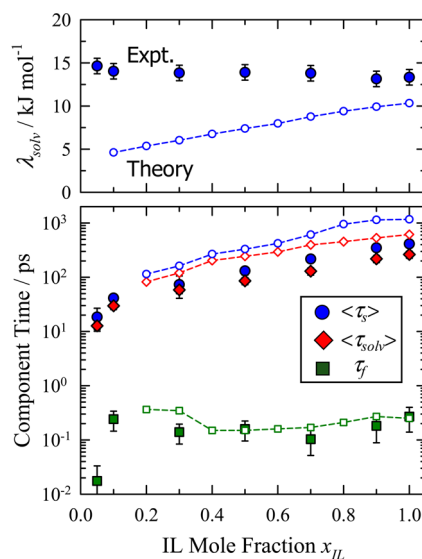


Figure 13. Comparison of observed reorganization energies and solvation times (filled symbols) with predictions of the semimolecular theory of Biswas and co-workers (connected open symbols).⁸⁶

independence observed experimentally. (In ref 86, Daschakraborty and Biswas noted that the unrealistically low value of λ_{solv} in water could be remedied by using the liquid-phase dipole moment of water (3.0 D) rather than the gas-phase value (1.8 D).) Much better qualitative agreement is found for the solvation time dependence. The solvation response functions predicted by the theory (not shown) are similar to those observed. They are comprised of a subpicosecond fast component associated with rapid reorientation of water and a slow, broadly distributed component involving cation reorientation and ion translations. The fast time constant (τ_f) predicted is close to what is observed experimentally (Figure 13) but the relative amplitude is significantly smaller than observed ($\sim 17\%$ versus $\sim 34\%$). The slow component in the theory is well represented by a stretched exponential time dependence having a stretching exponent averaging ~ 0.32 , somewhat smaller than observed ($\beta \sim 0.40$). The times of the slow component, $\langle \tau_s \rangle$, parallel the experimental times, and thus show the same fractional power dependence on viscosity that is observed in experiment. However, the predicted times are an average of 2.7-fold larger than those observed. Recall that the dielectric continuum model predicted times associated with the slower component of solvation which are too small by roughly a factor of 7 (Figure 10). Incorporation of molecular aspects of solvation in the theory of Biswas and co-workers thus improves agreement with experiment but apparently overcorrects the shortcomings of the continuum treatment.

4. SUMMARY AND CONCLUSIONS

We have presented new dielectric and solvation data in the prototypical mixture $[\text{Im}_{41}][\text{BF}_4] + \text{water}$. The measured permittivity and loss spectra undergo simple continuous evolution as functions of composition. The limiting permittivities, ϵ_∞ and ϵ , and the overall time constant associated with dielectric relaxation vary monotonically with IL mole (x_{IL}) or volume (Φ_{IL}) fraction, as do most other properties of this mixture. There is no evidence for abrupt structural changes taking place at particular compositions from any of the data examined here.

The absorption and steady-state emission spectra of coumarin 153 (C153) undergo only modest ($<600 \text{ cm}^{-1}$) shifts as functions of mixture composition. The solvation free energy change and reorganization energy associated with the $S_0 \leftrightarrow S_1$ transition of C153 vary by less than 15% as functions of composition and indicate slightly stronger solute–solvent interactions in the water-rich limit. The frequency shifts of C153 are weakly nonlinear functions of x_{IL} and strongly nonlinear functions of Φ_{IL} . On the basis of the simpler dependence of the dielectric properties measured here and the linear dependence of refractive index and ion density on Φ_{IL} , we suggest that volume fraction is the more appropriate variable with which to view solvation data. In this case, one might conclude that C153 is preferentially solvated by water in these mixtures. However, the complex relationship between spectral shifts and local environment in the presence of electrostatic interactions¹⁰³ renders any such conclusions highly suspect. Computer simulations will be required to adequately interpret the structural implications of solvatochromic measurements in this and similar mixtures.

The dynamic Stokes shifts of C153 at most compositions studied are similar to those observed in neat ionic liquids. The response is markedly biphasic. Initial solvation occurs via an ultrafast component with an amplitude of $\sim 34\%$ having a time constant of $\sim 0.2 \text{ ps}$ over the range $0.1 \leq x_{\text{IL}} \leq 1$. The slow

component of the response extends over the picosecond–nanosecond range, and its time-dependence can be represented by a stretched exponential function having an exponent near 0.4. Over most of the composition range ($0.1 \leq x_{\text{IL}} \leq 1$) the slow component time decreases with the addition of water in parallel with the solution viscosity in a manner consistent with a power law $\langle \tau_s \rangle \propto \eta^p$ with $p = 0.6$. The integral solvation time does not appear to be simply proportional to solution resistivity as predicted by simple dielectric continuum models.^{35,105} The dynamics observed at highest water content mixture studied, $x_{\text{IL}} = 0.05$ ($\Phi_{\text{IL}} = 0.35$), are distinctive. Here there is a very large ($\sim 60\%$) ultrafast component that cannot be resolved with the $\sim 80 \text{ fs}$ time resolution employed here, similar to the case in neat water. However, in contrast to water, in the ionic solution $\sim 20\%$ of the relaxation takes place on a much slower time scale of $\sim 20 \text{ ps}$.

The C153 data were compared to two theories connecting the solvent's dielectric response to time-dependent solvation. The first is the simple dielectric continuum theory, which has recently been tested in the case of a variety of neat ionic liquid solvents.²⁷ Similarly to what was found in neat ionic liquids, the simple dielectric continuum theory predicts solvation response functions that are qualitatively similar to but systematically faster than those observed, at least over the range $0.1 \leq x_{\text{IL}} \leq 1$. (At $x_{\text{IL}} = 0.05$ there are also qualitative differences.) Observed times average a factor of 7 larger than predictions, and differences between observed and predicted times tend to increase with decreasing x_{IL} . An alternative perspective on dielectric continuum modeling was provided by considering the dielectric dispersion and loss spectra required to reproduce the observed spectral response functions. The loss spectra so derived are similar to those measured experimentally, but the amplitudes ϵ_{eff} and σ_{eff} are on average smaller than experimental values by factors of 2 and 5, respectively. One can view the failure of dielectric continuum theory from this latter perspective as providing an effective dielectric response felt by the solute. Nevertheless, solvents are not continua, and apart from the luck achieved with conventional solvents, one does not expect a theory based on a dielectric continuum assumption to be quantitative. We also considered predictions of the only theory currently available that incorporates some molecular aspects of solvation, the semi-molecular theory of Biswas and co-workers.^{107,108,86} While this theory provides better agreement with observed solvation times, it appears to overcorrect the continuum theory, producing response functions that are uniformly too slow by a factor of ~ 3 . Hopefully, the comparisons afforded by the present data will encourage further refinement of this and other molecular theories.

■ ASSOCIATED CONTENT

Supporting Information

Plots of the composition dependence of dielectric parameters, viscosity data at 20.5°C , discussion of how spectral response data are fit, tabulated parameters of these fits, discussion of the approximations made for extrapolating dispersion data to higher frequencies than observed, and some direct comparisons between observed and predicted solvation response functions. This material is available free of charge via the Internet at <http://pubs.acs.org>.

■ AUTHOR INFORMATION

Corresponding Author

*E-mail: maroncelli@psu.edu.

Notes

The authors declare no competing financial interest.

ACKNOWLEDGMENTS

M.L. and M.M. were supported by the Division of Chemical Sciences, Geosciences, and Biosciences, Office of Basic Energy Sciences of the U.S. Department of Energy, through Grant DE-FG02-12ER16363, and J.H. and R.B. received support from the Deutsche Forschungsgemeinschaft (priority program "Ionic Liquids"). Experimental support was provided by N. P. Ernsting and his group, in part also funded by the Deutsche Forschungsgemeinschaft Ionic Liquids program. X.-X.Z. is grateful for support by the Humboldt University, and also by the Chinese Scholarship Council during earlier stages of this work.

REFERENCES

- (1) Stark, A. Ionic Liquid Structure-Induced Effects on Organic Reactions. *Top. Curr. Chem.* **2009**, *290*, 41–81.
- (2) Hallett, J. P.; Welton, T. Room-Temperature Ionic Liquids: Solvents for Synthesis and Catalysis. 2. *Chem. Rev.* **2011**, *111*, 3508–3576.
- (3) Wishart, J. F. Energy Applications of Ionic Liquids. *Energy Environ. Sci.* **2009**, *2*, 956–961.
- (4) Bakshiev, N. G. Universal Intermolecular Interactions and Their Effect on the Position of the Electronic Spectra of Molecules in Two-Component Solutions. *Opt. Spectrosc. (USSR)* **1964**, *16*, 446–451.
- (5) Ware, W. R.; Chow, P.; Lee, S. K. Time-Resolved Nanosecond Emission Spectroscopy: Spectral Shifts Due to Solvent-Solute Relaxation. *Chem. Phys. Lett.* **1968**, *2*, 356–358.
- (6) Maroncelli, M. The Dynamics of Solvation in Polar Liquids. *J. Mol. Liq.* **1993**, *57*, 1–37.
- (7) Stratt, R. M.; Maroncelli, M. Nonreactive Dynamics in Solution: The Emerging View of Solvation Dynamics and Vibrational Relaxation. *J. Phys. Chem.* **1996**, *100*, 12981–12996.
- (8) Bagchi, B.; Biswas, R. Polar and Nonpolar Solvation Dynamics, Ion Diffusion, and Vibrational Relaxation: The Role of Biphasic Solvent Response in Chemical Dynamics. *Adv. Chem. Phys.* **1999**, *109*, 207–433.
- (9) Rainieri, F. O.; Friedman, H. L. Solvent Control of Electron Transfer Reactions. *Adv. Chem. Phys.* **1999**, *107*, 81–189.
- (10) Richert, R. Triplet State Solvation Dynamics: Basics and Applications. *J. Chem. Phys.* **2000**, *113*, 8404–8429.
- (11) Horng, M. L.; Gardecki, J. A.; Papazyan, A.; Maroncelli, M. Sub-picosecond Measurements of Polar Solvation Dynamics: Coumarin 153 Revisited. *J. Phys. Chem.* **1995**, *99*, 17311–17337.
- (12) Sajadi, M.; Weinberger, M.; Wagenknecht, H.-A.; Ernsting, N. P. Polar Solvation Dynamics in Water and Methanol: Search for Molecularity. *Phys. Chem. Chem. Phys.* **2011**, *13*, 17768–17774.
- (13) Karmakar, R.; Samanta, A. Solvation Dynamics of Coumarin-153 in a Room-Temperature Ionic Liquid. *J. Phys. Chem. A* **2002**, *106*, 4447–4452.
- (14) Chakraborty, D.; Hazra, P.; Chakraborty, A.; Seth, D.; Sarkar, N. Dynamics of Solvent Relaxation in Room Temperature Ionic Liquids. *Chem. Phys. Lett.* **2003**, *381*, 697–704.
- (15) Funston, A. M.; Fadeeva, T. A.; Wishart, J. F.; Castner, E. W. Fluorescence Probing of Temperature-Dependent Dynamics and Friction in Ionic Liquid Local Environments. *J. Phys. Chem. B* **2007**, *111*, 4963–4977.
- (16) Jin, H.; Baker, G. A.; Arzhantsev, S.; Dong, J.; Maroncelli, M. Solvation and Rotational Dynamics of Coumarin 153 in Ionic Liquids: Comparisons to Conventional Solvents. *J. Phys. Chem. B* **2007**, *111*, 7291–7302.
- (17) Samanta, A. Solvation Dynamics in Ionic Liquids: What We Have Learned from the Dynamic Fluorescence Stokes Shift Studies. *J. Phys. Chem. Lett.* **2010**, *1*, 1557–1562.
- (18) Carlson, P. J.; Bose, S.; Armstrong, D. W.; Hawkins, T.; Gordon, M. S.; Petrich, J. W. Structure and Dynamics of the 1-Hydroxyethyl-4-amino-1,2,4-triazolium Nitrate High-Energy Ionic Liquid System. *J. Phys. Chem. B* **2012**, *116*, 503–512.
- (19) Song, X. Solvation Dynamics in Ionic Fluids: An Extended Debye-Huckel Dielectric Continuum Model. *J. Chem. Phys.* **2009**, *131*, 044503/044501–044508.
- (20) Daschakraborty, S.; Biswas, R. Ultrafast Solvation Response in Room Temperature Ionic Liquids: Possible Origin and Importance of the Collective and the Nearest Neighbour Solvent Modes. *J. Chem. Phys.* **2012**, *137*, 114501/114501–114511.
- (21) Shim, Y.; Kim, H. J. Dielectric Relaxation, Ion Conductivity, Solvent Rotation, and Solvation Dynamics in a Room-Temperature Ionic Liquid. *J. Phys. Chem. B* **2008**, *112*, 11028–11038.
- (22) Kobrak, M. N. A Comparative Study of Solvation Dynamics in Room-Temperature Ionic Liquids. *J. Chem. Phys.* **2007**, *127*, 184507/184501–184508.
- (23) Roy, D.; Maroncelli, M. Simulations of Solvation and Solvation Dynamics in an Idealized Ionic Liquid Model. *J. Phys. Chem. B* **2012**, *116*, 5951–5970.
- (24) Schröder, C.; Wakai, C.; Weingärtner, H.; Steinhäuser, O. Collective Rotational Dynamics in Ionic Liquids: A Computational and Experimental Study of 1-Butyl-3-methyl-imidazolium Tetrafluoroborate. *J. Chem. Phys.* **2007**, *126*, 84511.
- (25) Maroncelli, M.; Zhang, X.-X.; Liang, M.; Roy, D.; Ernsting, N. P. Measurements of the Complete Solvation Response of Coumarin 153 in Ionic Liquids and the Accuracy of Simple Dielectric Continuum Predictions. *Faraday Discuss.* **2012**, *154*, 409–424.
- (26) Halder, M.; Headley, L. S.; Mukherjee, P.; Song, X.; Petrich, J. W. Experimental and Theoretical Investigations of Solvation Dynamics of Ionic Fluids: Appropriateness of Dielectric Theory and the Role of DC Conductivity. *J. Phys. Chem. A* **2006**, *110*, 8623–8626.
- (27) Zhang, X.-X.; Liang, M.; Ernsting, N. P.; Maroncelli, M. Complete Solvation Response of Coumarin 153 in Ionic Liquids. *J. Phys. Chem. B* **2013**, *117*, 4291–4304.
- (28) Stoppa, A.; Hunger, J.; Buchner, R.; Hefter, G.; Thoman, A.; Helm, H. Interactions and Dynamics in Ionic Liquids. *J. Phys. Chem. B* **2008**, *112*, 4854–4858.
- (29) Turton, D. A.; Sonnleitner, T.; Ortner, A.; Walther, M.; Hefter, G.; Seddon, K. R.; Stana, S.; Plechkova, N. V.; Buchner, R.; Wynne, K. Structure and Dynamics in Protic Ionic Liquids: A Combined Optical Kerr-Effect and Dielectric Relaxation Spectroscopy Study. *Faraday Discuss.* **2012**, *154*, 145–153.
- (30) Krueger, M.; Bruendermann, E.; Funkner, S.; Weingaertner, H.; Havenith, M. Polarity Fluctuations of the Protic Ionic Liquid Ethylammonium Nitrate in the Terahertz Regime. *J. Chem. Phys.* **2010**, *132*, 101101/101101–101101/101104.
- (31) Arzhantsev, S.; Jin, H.; Baker, G. A.; Maroncelli, M. Measurements of the Complete Solvation Response in Ionic Liquids. *J. Phys. Chem. B* **2007**, *111*, 4978–4989.
- (32) Kimura, Y.; Fukuda, M.; Suda, K.; Terazima, M. Excited State Intramolecular Proton Transfer Reaction of 4'-N,N-Diethylamino-3-hydroxyflavone and Solvation Dynamics in Room Temperature Ionic Liquids Studied by Optical Kerr Gate Fluorescence Measurement. *J. Phys. Chem. B* **2010**, *114*, 11847–11858.
- (33) Lang, B.; Angulo, G.; Vauthey, E. Ultrafast Solvation Dynamics of Coumarin 153 in Imidazolium-Based Ionic Liquids. *J. Phys. Chem. A* **2006**, *110*, 7028–7034.
- (34) Liang, M.; Zhang, X.-X.; Kaintz, A.; Ernsting, N. P.; Maroncelli, M. Solvation and Solute Dynamics in Mixtures of 1-Butyl-3-Methylimidazolium Tetrafluoroborate and Acetonitrile. *J. Phys. Chem. B* **2013**, manuscript in preparation.
- (35) Zhang, X.-X.; Liang, M.; Ernsting, N. P.; Maroncelli, M. Conductivity and Solvation Dynamics in Ionic Liquids. *J. Phys. Chem. Lett.* **2013**, *4*, 1205–1210.
- (36) Stoppa, A.; Hunger, J.; Hefter, G.; Buchner, R. Structure and Dynamics of 1-N-Alkyl-3-N-Methylimidazolium Tetrafluoroborate + Acetonitrile Mixtures. *J. Phys. Chem. B* **2012**, *116*, 7509–7521.
- (37) Rebelo, L. P. N.; Najdanovic-Visak, V.; Visak, Z. P.; Nunes, d. P. M.; Szydłowski, J.; Cerdeirina, C. A.; Troncoso, J.; Romani, L.; Esperanca, J. M. S. S.; Guedes, H. J. R.; de, S. H. C. A Detailed

Thermodynamic Analysis of [C₄mim][BF₄] + Water as a Case Study to Model Ionic Liquid Aqueous Solutions. *Green Chem.* **2004**, *6*, 369–381.

(38) Katayanagi, H.; Nishikawa, K.; Shimozaki, H.; Miki, K.; Westh, P.; Koga, Y. Mixing Schemes in Ionic Liquid-H₂O Systems: A Thermodynamic Study. *J. Phys. Chem. B* **2004**, *108*, 19451–19457.

(39) Liu, W.; Zhao, T.; Zhang, Y.; Wang, H.; Yu, M. The Physical Properties of Aqueous Solutions of the Ionic Liquid [BMIM][BF₄]. *J. Sol. Chem.* **2006**, *35*, 1337–1346.

(40) Malham, I. B.; Turmine, M. Viscosities and Refractive Indices of Binary Mixtures of 1-Butyl-3-Methylimidazolium Tetrafluoroborate and 1-Butyl-2,3-Dimethylimidazolium Tetrafluoroborate with Water at 298 K. *J. Chem. Thermodyn.* **2008**, *40*, 718–723.

(41) Zhu, A.; Wang, J.; Han, L.; Fan, M. Measurements and Correlation of Viscosities and Conductivities for the Mixtures of Imidazolium Ionic Liquids with Molecular Solutes. *Chem. Eng. J.* **2009**, *147*, 27–35.

(42) Stoppa, A.; Hunger, J.; Buchner, R. Conductivities of Binary Mixtures of Ionic Liquids with Polar Solvents. *J. Chem. Eng. Data* **2009**, *54*, 472–479.

(43) Rilo, E.; Vila, J.; Pico, J.; Garcia-Garabal, S.; Segade, L.; Varela, L. M.; Cabeza, O. Electrical Conductivity and Viscosity of Aqueous Binary Mixtures of 1-Alkyl-3-methyl Imidazolium Tetrafluoroborate at Four Temperatures. *J. Chem. Eng. Data* **2010**, *55*, 639–644.

(44) Rilo, E.; Dominguez-Perez, M.; Vila, J.; Segade, L.; Garcia, M.; Varela, L. M.; Cabeza, O. Easy Prediction of the Refractive index for Binary Mixtures of Ionic Liquids with Water or Ethanol. *J. Chem. Thermodyn.* **2012**, *47*, 219–222.

(45) Taib, M. M.; Murugesan, T. Density, Refractive Index, and Excess Properties of 1-Butyl-3-methylimidazolium Tetrafluoroborate with Water and Monoethanolamine. *J. Chem. Eng. Data* **2011**, *57*, 120–126.

(46) Navarro, P.; Larriba, M.; Garcia, S.; Garcia, J.; Rodriguez, F. Physical Properties of Binary and Ternary Mixtures of 2-Propanol, Water, and 1-Butyl-3-methylimidazolium Tetrafluoroborate Ionic Liquid. *J. Chem. Eng. Data* **2012**, *57*, 1165–1173.

(47) Chen, Y.; Ke, F.; Wang, H.; Zhang, Y.; Liang, D. Phase Separation in Mixtures of Ionic Liquids and Water. *ChemPhysChem* **2012**, *13*, 160–167.

(48) Bowers, J.; Butts, C. P.; Martin, P. J.; Vergara-Gutierrez, M. C.; Heenan, R. K. Aggregation Behavior of Aqueous Solutions of Ionic Liquids. *Langmuir* **2004**, *20*, 2191–2198.

(49) Singh, T.; Kumar, A. Aggregation Behavior of Ionic Liquids in Aqueous Solutions: Effect of Alkyl Chain Length, Cations, and Anions. *J. Phys. Chem. B* **2007**, *111*, 7843–7851.

(50) Almasry, L.; Turmine, M.; Perera, A. Structure of Aqueous Solutions of Ionic Liquid 1-Butyl-3-methylimidazolium Tetrafluoroborate by Small-Angle Neutron Scattering. *J. Phys. Chem. B* **2008**, *112*, 2382–2387.

(51) Wu, B.; Liu, W. W.; Zhang, Y. M.; Wang, H. Do We Understand the Recyclability of Ionic Liquids? *Chem.—Eur. J.* **2009**, *15*, 1804–1810.

(52) Cammarata, L.; Kazarian, S. G.; Salter, P. A.; Welton, T. Molecular States of Water in Room Temperature Ionic Liquids. *Phys. Chem. Chem. Phys.* **2001**, *3*, 5192–5200.

(53) Fazio, B.; Triolo, A.; Marco, G. D. Local Organization of Water and Its Effect on the Structural Heterogeneities in Room-Temperature Ionic Liquid/H₂O mixtures. *J. Raman Spectrosc.* **2008**, *39*, 233–237.

(54) Jeon, Y.; Sung, J.; Kim, D.; Seo, C.; Cheong, H.; Ouchi, Y.; Ozawa, R.; Hamaguchi, H.-o. Structural Change of 1-Butyl-3-methylimidazolium Tetrafluoroborate + Water Mixtures Studied by Infrared Vibrational Spectroscopy. *J. Phys. Chem. B* **2008**, *112*, 923–928.

(55) Jeon, Y.; Sung, J.; Seo, C.; Lim, H.; Cheong, H.; Kang, M.; Moon, B.; Ouchi, Y.; Kim, D. Structures of Ionic Liquids with Different Anions Studied by Infrared Vibration Spectroscopy. *J. Phys. Chem. B* **2008**, *112*, 4735–4740.

(56) Chang, H.-C.; Jiang, J.-C.; Liou, Y.-C.; Hung, C.-H.; Lai, T.-Y.; Lin, S. H. Local Structures of Water in 1-Butyl-3-methylimidazolium Tetrafluoroborate Probed by High-Pressure Infrared Spectroscopy. *Anal. Sci.* **2008**, *24*, 1305–1309.

(57) Singh, T.; Kumar, A. Cation–Anion–Water Interactions in Aqueous Mixtures of Imidazolium Based Ionic Liquids. *Vib. Spectrosc.* **2011**, *55*, 119–125.

(58) Yoshimura, Y.; Kimura, H.; Okamoto, C.; Miyashita, T.; Imai, Y.; Abe, H. Glass Transition Behavior of Ionic Liquid, 1-Butyl-3-methylimidazolium Tetrafluoroborate-H₂O Mixed Solutions. *J. Chem. Thermodyn.* **2011**, *43*, 410–412.

(59) Mele, A.; Tran, C. D.; De, P. L. S. H. The Structure of a Room-Temperature Ionic Liquid With and Without Trace Amounts of Water: The Role of C–H...O and C–H...F Interactions in 1-*n*-Butyl-3-methylimidazolium Tetrafluoroborate. *Angew. Chem., Int. Ed.* **2003**, *42*, 4364–4366.

(60) Wu, B.; Liu, Y.; Zhang, Y.; Wang, H. Probing Intermolecular Interactions in Ionic Liquid–Water Mixtures by Near-Infrared Spectroscopy. *Chem.—Eur. J.* **2009**, *15*, 6889–6893.

(61) Schröder, C.; Hunger, J.; Stoppa, A.; Buchner, R.; Steinhauser, O. On the Collective Network of Ionic Liquid/Water mixtures. II. Decomposition and Interpretation of Dielectric Spectra. *J. Chem. Phys.* **2008**, *129*, 184501/184501–184501/184510.

(62) Dominguez-Vidal, A.; Kaun, N.; Ayora-Canada, M. J.; Lendl, B. Probing Intermolecular Interactions in Water/Ionic Liquid Mixtures by Far-Infrared Spectroscopy. *J. Phys. Chem. B* **2007**, *111*, 4446–4452.

(63) Koeberg, M.; Wu, C.-C.; Kim, D.; Bonn, M. THz Dielectric Relaxation of Ionic Liquid:Water Mixtures. *Chem. Phys. Lett.* **2007**, *439*, 60–64.

(64) Sturlaugson, A. L.; Fruchey, K. S.; Fayer, M. D. Orientational Dynamics of Room Temperature Ionic Liquid/Water Mixtures: Water-Induced Structure. *J. Phys. Chem. B* **2012**, *116*, 1777–1787.

(65) Shirota, H.; Biswas, R. Intermolecular/Interionic Vibrations of 1-Methyl-3-*n*-octylimidazolium Tetrafluoroborate Ionic Liquid and H₂O Mixtures. *J. Phys. Chem. B* **2012**, *116*, 13765–13773.

(66) Moreno, M.; Castiglione, F.; Mele, A.; Pasqui, C.; Raos, G. Interaction of Water with the Model Ionic Liquid [bmim][BF₄]: Molecular Dynamics Simulations and Comparison with NMR Data. *J. Phys. Chem. B* **2008**, *112*, 7826–7836.

(67) Schröder, C.; Rudas, T.; Neumayr, G.; Benkner, S.; Steinhauser, O. On the Collective Network of Ionic Liquid/Water Mixtures. I. Orientational Structure. *J. Chem. Phys.* **2007**, *127*, 234503/234501–234503/234509.

(68) Schröder, C.; Neumayr, G.; Steinhauser, O. On the Collective Network of Ionic Liquid/Water Mixtures. III. Structural Analysis of Ionic Liquids on the Basis of Voronoi Decomposition. *J. Chem. Phys.* **2009**, *130*, 194503/194501–194503/194511.

(69) Tian, G.; Li, J. Molecular Dynamics Simulation on the Structure and Dynamics of Water in the 1-Butyl-3-Methylimidazolium Tetrafluoroborate/Water Mixture. *J. Theor. Comput. Chem.* **2010**, *9*, 573–584.

(70) Zhong, X.; Fan, Z.; Liu, Z.; Cao, D. Local Structure Evolution and Its Connection to Thermodynamic and Transport Properties of 1-Butyl-3-methylimidazolium Tetrafluoroborate and Water Mixtures by Molecular Dynamics Simulations. *J. Phys. Chem. B* **2012**, *116*, 3249–3263.

(71) Sarkar, A.; Pandey, S. Solvatochromic Absorbance Probe Behavior and Preferential Solvation in Aqueous 1-Butyl-3-methylimidazolium Tetrafluoroborate. *J. Chem. Eng. Data* **2006**, *51*, 2051–2055.

(72) Sarkar, A.; Ali, M.; Baker, G. A.; Tetin, S. Y.; Ruan, Q.; Pandey, S. Multiprobe Spectroscopic Investigation of Molecular-Level Behavior within Aqueous 1-Butyl-3-methylimidazolium Tetrafluoroborate. *J. Phys. Chem. B* **2009**, *113*, 3088–3098.

(73) Trivedi, S.; Malek, N. I.; Behera, K.; Pandey, S. Temperature-Dependent Solvatochromic Probe Behavior within Ionic Liquids and (Ionic Liquid + Water) Mixtures. *J. Phys. Chem. B* **2010**, *114*, 8118–8125.

(74) Martins, C. T.; Sato, B. M.; El, S. O. A. First Study on the Thermo-solvatochromism in Aqueous 1-(1-Butyl)-3-methylimidazolium Tetrafluoroborate: A Comparison between the Solvation by an Ionic Liquid and by Aqueous Alcohols. *J. Phys. Chem. B* **2008**, *112*, 8330–8339.

(75) Kattinig, D. R.; Akdogan, Y.; Bauer, C.; Hinderberger, D. High-Field EPR Spectroscopic Characterization of Spin Probes in Aqueous

- Ionic Liquid Mixtures. *Z. Phys. Chem. (Muenchen, Ger.)* **2012**, *226*, 1363–1377.
- (76) Kattinig, D. R.; Hinderberger, D. Temperature-Dependent Formation and Transformation of Mesostuctures in Water–Ionic Liquid Mixtures. *Chem.—Asian J.* **2012**, *7*, 1000–1008.
- (77) Baker, S. N.; Baker, G. A.; Munson, C. A.; C., F.; Bukowski, E. J.; Cartwright, A. N.; Bright, F. V. Effects of Solubilized Water on the Relaxation Dynamics Surrounding PRODAN Dissolved in 1-Butyl-3-imidazolium Hexafluorophosphate at 298 K. *Ind. Eng. Chem. Res.* **2003**, *42*, 6457–6463.
- (78) Chakraborty, D.; Chakraborty, A.; Seth, D.; Hazra, P.; Sarkar, N. Dynamics of Solvation and Rotational Relaxation of Coumarin 153 in 1-Butyl-3-methylimidazolium Hexafluorophosphate [bmim][PF₆]–Water Mixtures. *Chem. Phys. Lett.* **2004**, *397*, 469–474.
- (79) Chakraborty, D.; Chakraborty, A.; Seth, D.; Sarkar, N. Effect of Water, Methanol, and Acetonitrile on Solvent Relaxation and Rotational Relaxation of Coumarin 153 in Neat 1-Hexyl-3-methylimidazolium Hexafluorophosphate. *J. Phys. Chem. A* **2005**, *109*, 1764–1769.
- (80) Pramanik, R.; Rao, V. G.; Sarkar, S.; Ghatak, C.; Setua, P.; Sarkar, N. To Probe the Interaction of Methanol and Acetonitrile with the Ionic Liquid *N,N,N*-Trimethyl-*N*-propyl Ammonium Bis-(trifluoromethanesulfonyl) Imide at Different Temperatures by Solvation Dynamics Study. *J. Phys. Chem. B* **2009**, *113*, 8626–8634.
- (81) Sarkar, S.; Pramanik, R.; Ghatak, C.; Setua, P.; Sarkar, N. Probing the Interaction of 1-Ethyl-3-methylimidazolium Ethyl Sulfate ([Emim]-[EtSO₄]) with Alcohols and Water by Solvent and Rotational Relaxation. *J. Phys. Chem. B* **2010**, *114*, 2779–2789.
- (82) Paul, A.; Samanta, A. Effect of Nonpolar Solvents on the Solute Rotation and Solvation Dynamics in an Imidazolium Ionic Liquid. *J. Phys. Chem. B* **2008**, *112*, 947–953.
- (83) Das, S. K.; Sarkar, M. Steady-State and Time-Resolved Fluorescence Behavior of Coumarin-153 in a Hydrophobic Ionic Liquid and Ionic Liquid–Toluene Mixture. *J. Mol. Liq.* **2012**, *165*, 38–43.
- (84) Kimura, Y.; Kobayashi, A.; Demizu, M.; Terazima, M. Solvation Dynamics of Coumarin 153 in Mixtures of Carbon Dioxide and Room Temperature Ionic Liquids. *Chem. Phys. Lett.* **2011**, *513*, 53–58.
- (85) Annappureddy, H. V. R.; Hu, Z.; Xia, J.; Margulis, C. J. How Does Water Affect the Dynamics of the Room-Temperature Ionic Liquid 1-Hexyl-3-methylimidazolium Hexafluorophosphate and the Fluorescence Spectroscopy of Coumarin-153 When Dissolved in It? *J. Phys. Chem. B* **2008**, *112*, 1770–1776.
- (86) Daschakraborty, S.; Biswas, R. Stokes Shift Dynamics in (Ionic Liquid + Polar Solvent) Binary Mixtures: Composition Dependence. *J. Phys. Chem. B* **2011**, *115*, 4011–4024.
- (87) Buchner, R.; Hefter, G. T.; May, P. M. Dielectric Relaxation of Aqueous NaCl Solutions. *J. Phys. Chem. A* **1999**, *103*, 1–9.
- (88) Barthel, J.; Bachhuber, K.; Buchner, R.; Hetzenauer, H.; Kleebauer, M. A Computer-Controlled System of Transmission Lines for the Determination of the Complex Permittivity of Lossy Liquids between 8.5 and 90 GHz. *Ber. Bunsen-Ges. Phys. Chem.* **1991**, *95*, 853–859.
- (89) Schroedle, S.; Hefter, G.; Kunz, W.; Buchner, R. Effects of Nonionic Surfactant C12E5 on the Cooperative Dynamics of Water. *Langmuir* **2006**, *22*, 924–932.
- (90) Gardecki, J. A.; Maroncelli, M. A Set of Secondary Emission Standards for Calibration of Spectral Responsivity in Emission Spectroscopy. *Appl. Spectrosc.* **1998**, *52*, 1179–1189.
- (91) Maroncelli, M.; Fleming, G. R. Picosecond Solvation Dynamics of Coumarin 153: The Importance of Molecular Aspects of Solvation. *J. Chem. Phys.* **1987**, *86*, 6221–6239.
- (92) Zhang, X. X.; Wurth, C.; Zhao, L.; Resch-Genger, U.; Ernsting, N. P.; Sajadi, M. Femtosecond Broadband Fluorescence Upconversion Spectroscopy: Improved Setup and Photometric Correction. *Rev. Sci. Instrum.* **2011**, *82*, 063108.
- (93) Wakai, C.; Oleinikova, A.; Ott, M.; Weingaertner, H. How Polar Are Ionic Liquids? Determination of the Static Dielectric Constant of an Imidazolium-based Ionic Liquid by Microwave Dielectric Spectroscopy. *J. Phys. Chem. B* **2005**, *109*, 17028–17030.
- (94) Nakamura, K.; Shikata, T. Systematic Dielectric and NMR Study of the Ionic Liquid 1-Alkyl-3-Methyl Imidazolium. *ChemPhysChem* **2010**, *11*, 285–294.
- (95) Hunger, J.; Stoppa, A.; Schroedle, S.; Hefter, G.; Buchner, R. Temperature Dependence of the Dielectric Properties and Dynamics of Ionic Liquids. *ChemPhysChem* **2009**, *10*, 723–733.
- (96) Huang, M.-M.; Jiang, Y.; Sasisanker, P.; Driver, G. W.; Weingartner, H. Static Relative Dielectric Permittivities of Ionic Liquids at 25 °C. *J. Chem. Eng. Data* **2011**, *56*, 1494–1499.
- (97) The data of Liu et al.³⁹ systematically deviate from the other data (and our own unpublished values) and were omitted from the viscosity fit. The refractive index data in that same paper also deviate substantially from the data shown in Figure 2 and was also not included. Likewise, the conductivity data of Zhu et al.⁴¹ were omitted from the fits.
- (98) Woodward, C. E.; Harris, K. R. A Lattice-Hole Theory for Conductivity in Ionic Liquid Mixtures: Application to Ionic Liquid + Water Mixtures. *Phys. Chem. Chem. Phys.* **2010**, *12*, 1172–1176.
- (99) Fee, R. S.; Maroncelli, M. Estimating the Time-Zero Spectrum in Time-Resolved Emission Measurements of Solvation Dynamics. *Chem. Phys.* **1994**, *183*, 235–247.
- (100) Marcus, Y. *Solvent Mixtures, Properties and Selective Solvation*; Marcel-Dekker: New York, 2002.
- (101) Mellein, B. R.; Aki, S. N. V. K.; Ladewski, R. L.; Brennecke, J. F. Solvatochromic Studies of Ionic Liquid/Organic Mixtures. *J. Phys. Chem. B* **2007**, *111*, 131–138.
- (102) Reichardt, C. Solvatochromic Dyes as Solvent Polarity Indicators. *Chem. Rev.* **1994**, *94*, 2319–2358.
- (103) Li, H.; Arzhantsev, S.; Maroncelli, M. Solvation and Solvatochromism in CO₂-Expanded Liquids. 2. Experiment-Simulation Comparisons of Preferential Solvation in Three Prototypical Mixtures. *J. Phys. Chem. B* **2007**, *111*, 3208–3221.
- (104) Jimenez, R.; Fleming, G. R.; Kumar, P. V.; Maroncelli, M. Femtosecond Solvation Dynamics of Water. *Nature* **1994**, *369*, 471–473.
- (105) Zhang, X.-X.; Schröder, C.; Ernsting, N. P. Solvation and Dielectric Response in Ionic Liquids – Conductivity Extension of the Continuum Model. *J. Chem. Phys.* **2013**, *138*, 111102/111101–111103.
- (106) Ellison, W. J. Permittivity of Pure Water, at Standard Atmospheric Pressure, Over the Frequency Range 0–25 THz and the Temperature Range 0–100 °C. *J. Phys. Chem. Ref. Data* **2007**, *36*, 1–18.
- (107) Kashyap, H. K.; Biswas, R. Dipolar Solvation Dynamics in Room Temperature Ionic Liquids: An Effective Medium Calculation Using Dielectric Relaxation Data. *J. Phys. Chem. B* **2008**, *112*, 12431–12438.
- (108) Kashyap, H. K.; Biswas, R. Solvation Dynamics in Imidazolium and Phosphonium Ionic Liquids: Effects of Solute Motion. *Indian J. Chem., Sect. A: Inorg., Bio-inorg., Phys., Theor. Anal. Chem.* **2010**, *49A*, 685–694.